Desalination and Water Treatment
www.deswater.com

doi: 10.1080/19443994.2013.817508

52 (2014) 6230–6239
September

Taylor & Francis
Taylor & Francis Group

Rapid purification of spent pickling liquor into ferrite by microwave hydrothermal method

Dan Chen*, Yun Guo, Yang Li

School of Environmental and Chemical Engineering, Shanghai University, No. 99 ShangDa Road, BaoShan District, Shanghai, China
Tel. +86 21 66137784; Fax: +86 21 66137756; email: dchen@shu.edu.cn

Received 6 May 2012; Accepted 30 May 2013

ABSTRACTS

Spinel ferrite was synthesized from two kinds of spent pickling liquor (SPL) by microwave hydrothermal method. X-ray diffraction (XRD) and toxicity characteristic leaching procedure (TCLP) showed that the synthesized product (V_{SPLA}:$V_{\mathrm{SPLB}} = 1$:1) was well crystallized as well as had relatively high saturation magnetization (48.57 emu/g) and BET surface area (76.67 $\mathrm{m^2/g}$). Scanning electron microscope (SEM) and transmission electron microscope (TEM) revealed ferrite nanoparticles in size of around 20 nm. An adsorption experiment indicated that the obtained product was a kind of efficient and powerful magnetic adsorbent for the removal of methylene blue (MB) from aqueous solution. The effect of contact time, solution pH, and initial concentration was investigated. Adsorption kinetics data followed the pseudo-second-order model and adsorption isotherm data were fitted well to the Langmuir model with a maximum MB adsorption capacity of 33.07 $\mathrm{mg\,g^{-1}}$. Furthermore, higher reaction temperature was beneficial for larger grain size and better crystallinity of the particle. The activation energy of ferrite process was 5.54 kJ/mol, which was much lower than that of other methods. Thus, microwave hydrothermal method was an environmentally friendly and economic process to realize two kinds of spent pickling liquor co-treatment.

Keywords: Spent pickling liquor; Spinel ferrite; Grain growth; Adsorption

1. Introduction

During the hot rolling or heat treatment of steel, oxygen from the atmosphere reacts with the iron on the surface of the steel form a mixture of iron oxides crust. In order to make subsequent process operate successfully, the presence of oxide on the surface should be removed by various acids such as HCl, HNO_3, HF, or H_2SO_4. Spent pickling liquor from pickling of different surfaces is considered as hazardous waste. It not only corrodes metals and concrete sewage pipes, but also is harmful to the ecosystem, if it is discharged with abandon. Besides, the precipitates after simply neutralization are unstable and hazardous metals such as Cu, Fe, and Ni can be easily leached out [1].

Ferrite general formula can be expressed as XY_2O_4, where X is divalent ion (Mg^{2+}, Fe^{2+}, Mn^{2+}, Ni^{2+}, or Zn^{2+}) or their combination, Y mainly stands for Fe^{3+} but can be substituted by any trivalent ions (Al^{3+} and Cr^{3+}) [2]. It is known that ferrite is used widely in applications such as gas sensing [3] and catalytic

---

*Corresponding author.

applications [4]. In recent years, owing to its effective magnetic separation, ferrite can be used as the adsorbent to treat organic dyes wastewater [5].

Ferrite process can be considered as an efficient way to treat industrial wastes such as electroplating sludge or wastewater. During the process, metals in the wastewater can be fixed well in the crystal lattice of ferrite [6,7]. Generally, ferrite process requires proper metals ratio (X:Y = 1:2) to form ferrite. However, this molar ratio is hard to achieve in actual wastewater systems. Thus, it is necessary to add additional metal ions to supplement the shortage.

There are various methods to synthesize spinel ferrite, in comparison, microwave hydrothermal method has obvious advantages, which is fast-heating and homogeneous temperature gradient as well as needs low activation energy [8–9]. Thus, this study is focused on: (1) realizing co-treatment of two kinds of spent pickling liquors and synthesis of spinel ferrite by microwave hydrothermal method; (2) investigating the grain growth activation energy and confirming the efficiency of microwave hydrothermal method in this wastewater system; and (3) using the synthesized ferrite as a magnetic adsorbent to remove methylene blue (MB) from aqueous solution.

2. Experimental

2.1. Materials

Spent pickling liquor SPL_A and SPL_B was provided by Shanghai Hazardous Waste Management Centre (Shanghai, China) and Shanghai Yingshengshiye Co., Ltd, respectively. The contents of heavy metals are shown in Table 1. NaOH, HCl, acetic acid, and sodium acetate were brought from Sinopharm Group Chemical Reagent Co., Ltd. with analytical grade and used as supplied.

2.2. Preparation of ferrite by microwave hydrothermal method

Two kinds of typical spent pickling liquors were mixed together according to different wastewater volume ratios, and pH value was adjusted to 11 with NaOH (5 M) to obtain precursors. The precursors were put into Teflon liner reactors, then transferred to the microwave digestion system (WX-4000, Shanghai Yi-Yao Instruments, China) and heated (150˚C, 30 min) [9]. Then the products were filtered to separate solid from liquid and then cooled naturally. Precipitates were washed by deionized water 4–6 times and dried at 80˚C overnight and finally powdered.

Table 1
Contents of main metals in spent pickling liquor

Spent pickling liquor	Metal concentration (g/L)				
	Cu	Fe	Ni	Cr	Zn
SPL_A	0.4	103.14*	0.23	0.29	UD
SPL_B	0.06	30.15[a]	3.35	3.33[b]	0.01

[a]Fe(III). [b]Cr(III).*Fe(III)-4.24 g/L, Fe(II)-98.9 g/L
UD related to undetected.

2.3. Tclp

Toxicity characteristic leaching procedure (TCLP) was used to determine the chemical stability of the synthesized products [10]. The solutions with pH of 2.88 ± 0.05 (leaching reagent A) and 4.93 ± 0.05 (leaching reagent B) were chosen as the leaching reagent. The ratio of solid to liquid was 1:20. The samples were rotated at the rate of 30 ± 2 rpm for 18 h, and filtrated after undisturbed placement for half an hour. The filtrate was kept in a plastic bottle for the toxicity analysis of heavy metal.

2.4. Characterization

The liquid was chemically analyzed by inductively coupled plasma atom emission spectrometer (ICP-AES) (Leeman Co., USA). The detection limit of each heavy metal is as follows: Ni 0.04 mg/L, Cu 0.03 mg/L, Cr 0.05 mg/L, Zn 0.04 mg/L, and Fe 0.07 mg/L. Synthesized solids were characterized by X-ray diffraction (XRD) with Cu Kα radiation (40 kV to 40 mA, model: D/MAX-2200X, Japan). Vibrating Sample Magnetometer (VSM) (7407 type, LakeShore Company, USA) was used to measure magnetic properties of the synthesized products. The specific surface area was evaluated on N_2 adsorption measurement (Quadrasorb SI, Quantachrome company, USA) with Brunauer–Emmett–Teller (BET) method. The morphology image of the ferrite was taken on the scanning electron microscope (SEM, JEOLJSM6700) with gold coating and transmission electron microscope (TEM, Hitachi H-800). The sample for TEM was prepared by dispersing the powder in ethanol and coating a very dilute suspension on carbon-coated Cu grids. The equilibrium concentration of Methylene Blue in adsorption experiment was analyzed by UV–visible spectrophotometer (Model, EL96043181) at 665 nm. The solution pH was adjusted with using a PHS-3C pH meter.

2.5. Adsorption experiments

About 0.2 g adsorbent and 50 mL MB solution (50 mg/L) were transferred in glass vessels and agitated by vigorous stirring at room temperature. At a defined time interval, the equilibrium concentrations of the solutions were examined by using linear regression equation ($y = 0.204x - 0.002$, $R^2 = 0.999$). The adsorption capacity was calculated according to Eq. (1).

$$q = \frac{(C_0 - C_e)V}{m} \tag{1}$$

where q (mg/g) is the adsorption capacity; C_0 (mg/L) and C_e (mg/L) are initial and equilibrated MB concentrations, respectively; V (L) is the volume of added solution; and m (g) is the mass of the adsorbent (dry).

3. Results and discussion

3.1. Ferrite process during the treatment of spent pickling liquor

In order to confirm the metastasis of metal ions from spent pickling liquor into the precipitation phase and the occurrence of ferrite process, the concentrations of metals in supernatant were measured and precipitated phase was analyzed by XRD. Concentrations of metals with different wastewater volume ratios in supernatant are listed in Table 2. A large amount of metals remained in the supernatant without adding SPL_A. Cu, Fe, Ni, and Cr ions concentrations were 20.58 mg/L, 16.54 mg/L, 7.99 mg/L, and 50.97 mg/L, respectively. With the increasing of the SPL_A volume, the concentrations of metals in supernatant began to decrease obviously. Only 2.96 mg/L Cr ions remained in treated supernatant (V_{SPLA}:$V_{SPLB} = 1{:}1$), which indicated that the metals in the liquid phase had transferred into the solid phase.

The XRD patterns of the prepared solids are shown in Fig. 1. The final products were mainly Na_3FSO_4 and $FeCO_3$ without adding SPL_A. It can be seen that the intensity of spinel diffraction peaks was almost visible in the case of V_{SPLA}:$V_{SPLB} = 1{:}5$ and increased with increasing volume of SPL_B. Ferrite process without sufficient divalent ions may result in poor crystallization and low stability of the ferrite [11]. In other words, increasing the volume of SPL_B (divalent ions) is more favorable for formation of spinel ferrites. Fig. 1(g) shows that the product crystallized well and without any other detectable solid phases. Thus, the wastewater volume ratio of 1:1 was appropriate to obtain spinel ferrite.

Table 2
Effect of wastewater volume ratios on supernatant and stability of products (mg/L)

Samples V_{SPLA}:V_{SPLB}	Conditions	Metal concentration (mg/L)				
		Cu	Fe	Ni	Cr	Zn
Without SPL_A	Supernatant	20.58	16.54	7.99	50.97	UD
	TCLP results in leaching reagent B	UD	12.09	7.5	22.46	UD
	TCLP results in leaching reagent A	UD	8.80	71.11	49.55	UD
1:6	Supernatant	15.21	14.24	8.16	44.59	UD
	TCLP results in leaching reagent B	UD	5.61	11.13	21.79	UD
	TCLP results in leaching reagent A	UD	6.29	62.83	32.58	UD
1:5	Supernatant	UD	15.57	7.82	17.97	UD
	TCLP results in leaching reagent B	UD	UD	73.75	UD	UD
	TCLP results in leaching reagent A	UD	0.61	124.97	1.23	UD
1:4	Supernatant	UD	UD	UD	9.15	UD
	TCLP results in leaching reagent B	UD	UD	73.12	UD	UD
	TCLP results in leaching reagent A	UD	0.33	118.94	0.87	UD
1:3	Supernatant	UD	UD	UD	6.00	UD
	TCLP results in leaching reagent B	UD	UD	74.96	UD	UD
	TCLP results in leaching reagent A	UD	0.58	129.30	0.79	UD
1:2	Supernatant	UD	UD	UD	5.98	UD
	TCLP results in leaching reagent B	UD	UD	UD	UD	UD
	TCLP results in leaching reagent A	UD	UD	58.60	UD	UD
1:1	Supernatant	UD	UD	UD	2.96	UD
	TCLP results in leaching reagent B	UD	UD	UD	UD	UD
	TCLP results in leaching reagent A	UD	UD	8.09	UD	UD
TCLP standard		15	–	–	5	–

UD related to undetected.

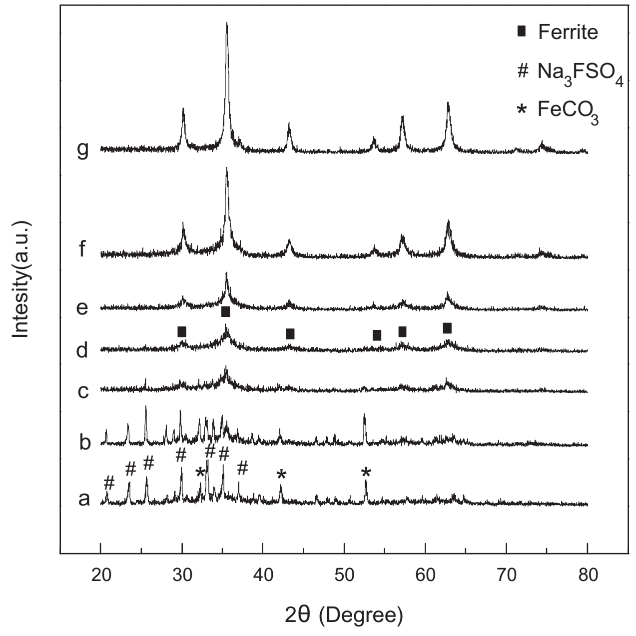

Fig. 1. XRD patterns of samples with different wastewater volume ratios V_{SPLA}:V_{SPLB} = (a) without SPL_A, (b) 1:6, (c) 1:5, (d) 1:4, (e) 1:3, (f) 1:2, and (g) 1:1.

3.2. Tclp

TCLP is usually used to evaluate the environmental leaching risk of solid waste. The waste will be classified as the hazardous waste, if the concentration of pollutants extracted exceeds regulatory limit. The leaching concentrations of heavy metals are listed in Table 2. There were 49.55 mg/L and 22.46 mg/L of Cr ions in the solution after TCLP without adding SPL_A. This leaching concentration exceeded TCLP standard limit, suggesting that the final solids were unstable. While it can be noticed that Cr ions leaching concentrations dropped sharply with the growth of SPL_A volume and could not be detected in leaching solution at V_{SPLA}:V_{SPLB} = 1:1. In comparison, Ni ions leached out more heavily with the maximum leaching concentration of 129.30 mg/L due to the poor crystallization and low stability of the product. However, there were a few Ni ions leached out even at the well-crystalline structure of the ferrite (8.09 mg/L). This may be due to ion competition during the ferrite process. Generally, Ni ions were less competitive to enter lattice sites of ferrite compared with Fe and Cr ions. Thus, a small part of Ni ions might be adsorbed on the surface of the final solid products actually and they would be washed out in severe acid condition.

Fig. 2(a) shows the XRD pattern of the ferrite (V_{SPLA}:V_{SPLB} = 1:1) after TCLP in leaching reagent A. As can be seen, the characteristic peaks did not change obviously, confirming that the heavy metals which fixed into the lattice of the spinel structure belong to chemical stable species and even TCLP test cannot make them mobile [12].

3.3. Magnetization, BET surface area, and morphology

The magnetization measurement for the prepared ferrite (V_{SPLA}:V_{SPLB} = 1:1) was carried out at room temperature with an applied magnetic field. The ferrite exhibited a well soft magnetic property (b in

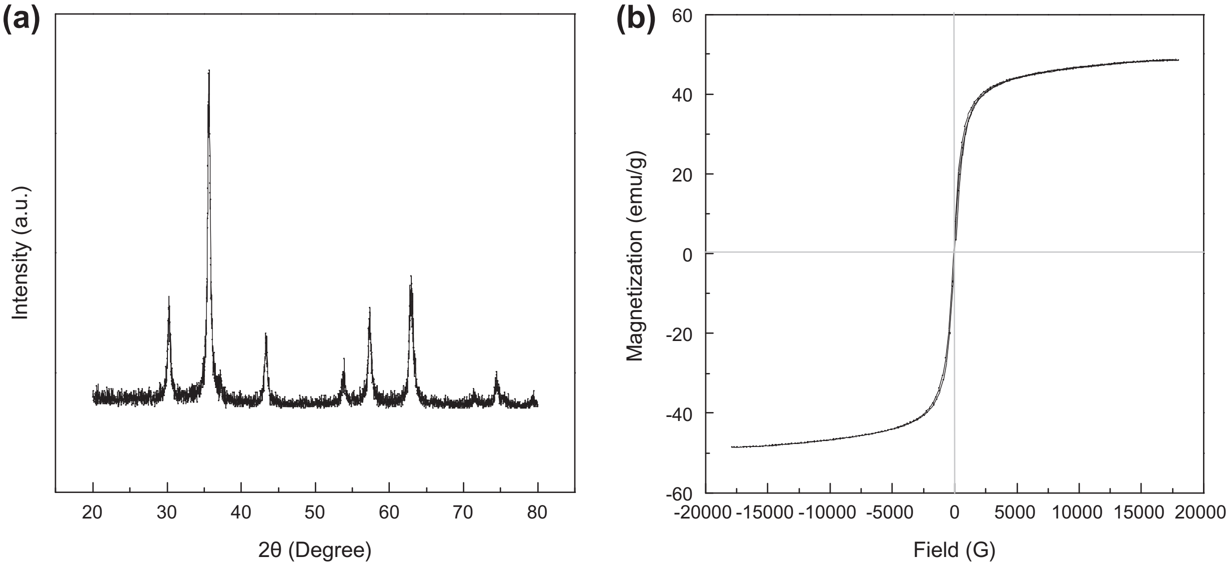

Fig. 2. (a) XRD patterns of synthesized ferrite after TCLP and (b) magnetization characteristic curve (V_{SPLA}:V_{SPLB} = 1:1).

Fig. 2) and had values of coercivity (Hc), saturation magnetization (Ms), and remnant magnetization (Mr) of about 95.38 G, 48.57 emu/g, and 6.02 emu/g, respectively. BET surface areas calculated from nitrogen adsorption isotherm plot are displayed in Table 3. The total pore volume (0.18 cm^3/g) was relatively high, and the BET surface area (76.67 m^2/g) was much larger than that of $Mn_{1-x}Zn_xFe_2O_4$ samples (20.65–29.80 m^2/g) reported by Hou et al. [13].

The scanning electron microscopy (SEM) micrograph for obtained ferrite (V_{SPLA}:V_{SPLB} = 1:1) is displayed in Fig. 3(a). It can be seen the fine and homogenous nanospheres of ferrite particles contained some agglomeration. The agglomeration of particles is related with many factors such as shape factor, surface area, and porosity [14]. Transmission electron microscopy (TEM) is shown in Fig. 3(b), which provides further insight into the morphologies and structural details of the system. The TEM image shows rather rough spherical nanoparticles with an average size of 20 nm.

3.4. *Grain growth kinetics and activation energy*

Fig. 4 shows XRD patterns of samples prepared at various temperatures ranging from 90°C to 210°C with the retention time 60 min. It can be seen that the spinel diffraction peaks were considerably broadening and weak at lower temperature, indicating the small-sized particle nature of the ferrite powder. The intensity of the spinel peaks was obviously increased with increasing the reaction temperature. The average grain size for each sample was calculated by Scherrer formula [15] according to the most intense peak (3 1 1).

$$D = \frac{0.9\lambda}{\beta \cos\theta} \tag{2}$$

where D is the average crystalline size, λ is the wavelength of Cu Kα, β is the full width at half maximum (FWHM) of the diffraction peaks, and θ is the Bragg's angle. With the temperature rising from 90°C to 210°C, the grain size grew from 18.4 to 29.3 nm, increasing by 59.2%. Thus, it confirmed that high temperature could greatly favor a particle with larger grain sizes and a better crystallinity [16]. The reason for the flash reaction velocity of the microwave hydrothermal process might be its flash rising temperature.

Table 3
Magnetization, BET surface area, and total pore volume of synthesized ferrite

Sample (V_{SPLA}:V_{SPLB} = 1:1)	Ferrite
Saturation magnetization (emu/g)	48.57
Coercivity (G)	95.38
Remnant magnetization (emu/g)	6.02
BET-surface area (m^2/g)	76.67
Total pore volume (cm^3/g)	0.18

The activation energy of grain growth can be calculated by the Arrhenius equation:

$$\frac{d \ln k}{dT} = \frac{Q}{RT^2} \tag{3}$$

where k is the specific reaction rate constant, Q is the activation energy, T is the absolute temperature, and R is the ideal gas constant. And Eq. (3) can be transformed to Eq. (4):

$$\log D = -\frac{Q}{2.303RT} + A \tag{4}$$

where D is the grain size and A is the intercept. Eq. (4) made a plot of $\log D$ vs. the reciprocal of absolute temperature ($1/T$) and obtained a straight-line plot of the grain size (Fig. 5). The plot gives a correlation with correlation coefficient $R^2 = 0.900$. The slope of the resulting Arrhenius plot was $-Q/2.303R$ and the calculated activation energy of grain growth was about 5.54 kJ/mol. Mn–Zn ferrite synthesized by high energy consuming sinter process needed 71.14 kJ/mol activation energy [17]. Ni–Zn ferrite prepared by conventional hydrothermal method had 41.6 kJ/mol activation energy [18]. Compared with these high energy consuming technologies, microwave hydrothermal method can be seen as an economical process.

3.5. *Application in MB adsorption*

3.5.1. *Characterization of MFLA after adsorption*

The synthesized ferrite (V_{SPLA}:V_{SPLB} = 1:1) was chosen as the adsorbent for the adsorption experiment. The effect of contact time on the adsorbed amount of MB was investigated (Fig. 6). As can be seen, the rate of adsorption increased rapidly during the initial adsorption stage (5 min) and reached equilibrium after 40 min. The inset photograph in Fig. 6 confirms that the adsorbent can be recycled by magnet after MB adsorption. In the past, using traditional adsorbents like active carbon, might cause some problems such as the blockage of filters or the loss of adsorbents [19]. However, this magnetic adsorbent could easily overcome these disadvantages.

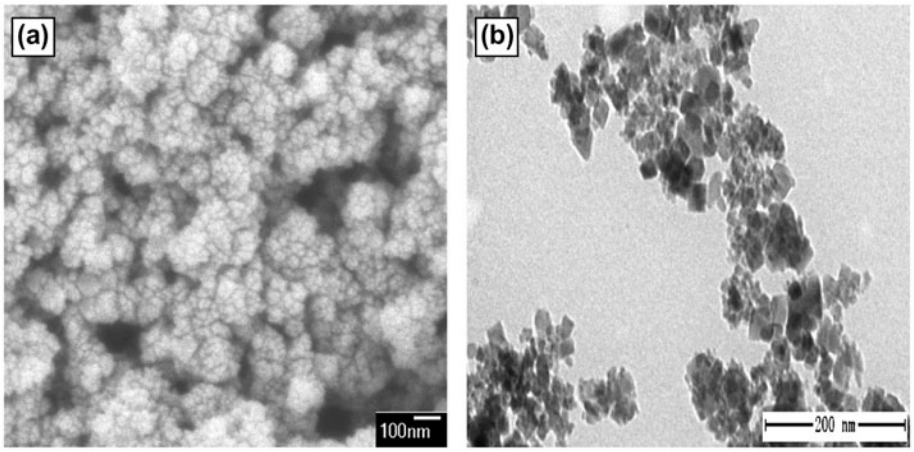

Fig. 3. SEM (a) and TEM (b) images of synthesized ferrite (V_{SPLA}:V_{SPLB} = 1:1).

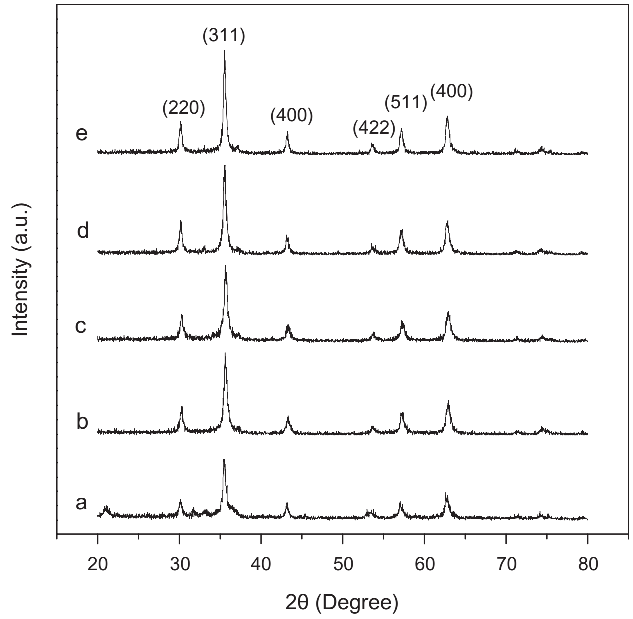

Fig. 4. XRD patterns of materials synthesized with different temperatures: (a) 90℃; (b) 120℃; (c) 150℃; (d) 180℃; and (e) 210℃.

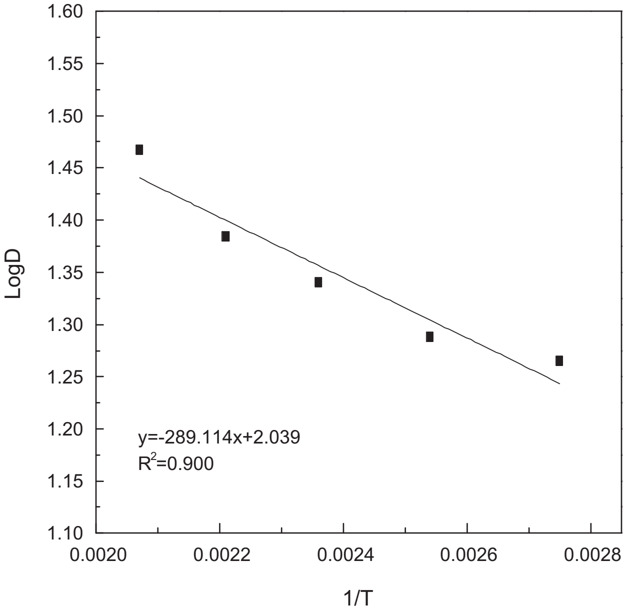

Fig. 5. Plots of log D vs. the reciprocal of absolute temperature (1/T).

A rapid adsorption rate and excellent characterization suggested that the ferrite is a potential and promising adsorbent to treat dye wastewater.

FTIR analysis on ferrite before and after MB adsorption process is presented in Fig. 7. The peak at 3420.74–3433.37 cm^{-1} and 1598.47–1634.51 cm^{-1} was attributed to the H–O–H bending vibration of water. The bands at 590.37 cm^{-1} and 472.91 cm^{-1} correspond to tetrahedral and octahedral sites of spinel ferrite, respectively. There was a weak band at 1382.01 cm^{-1} and 1391.24 cm^{-1} which was asymmetric NO_3^- stretching vibration arising from the residual nitrate groups. It can be noticed that five new peaks at 2375.53 cm^{-1}, 1470.75 cm^{-1}, 1154.84 cm^{-1}, 927.22 cm^{-1}, and 827.05 cm^{-1} appeared after MB adsorption. This might be attributed to the functional groups of MB (C=O, C=C, C–O, and C–H) adsorbed on to the ferrite. It can be noticed that other peaks shifted or strengthened after the reaction as well. These changes could indicate the chemical bonds, $–N^+(CH_3)_2$ of MB cations and Fe–O bond of ferrite were responsible for the electrostatic attraction onto the adsorbent [20,21].

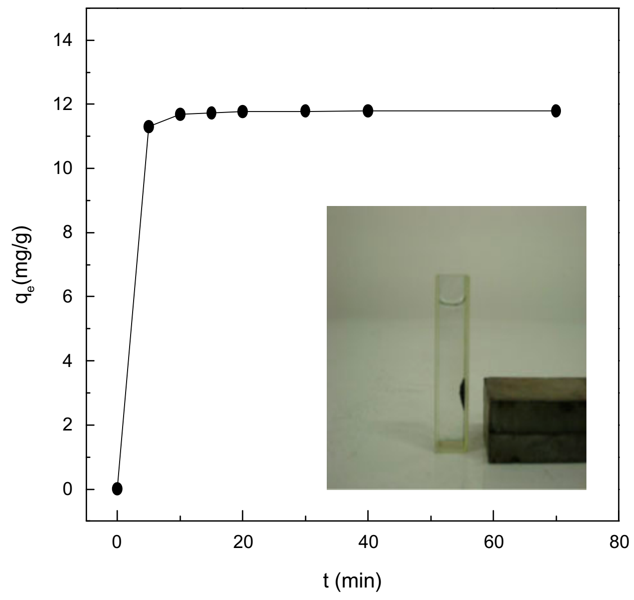

Fig. 6. Adsorption kinetics of MB adsorption with 50 mg/L.

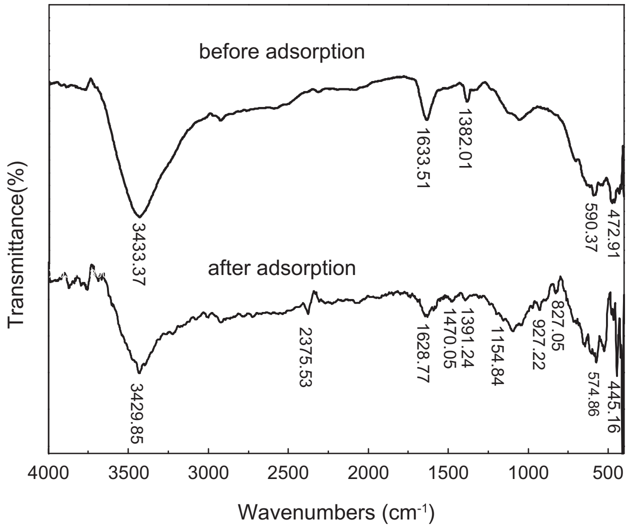

Fig. 7. FTIR of ferrite before and after MB adsorption.

3.5.2. Effect of initial pH

It is known that the pH of the dye solution plays an important part in the adsorption process [22]. The effect of pH on the adsorption of MB by ferrite was performed at pH 2–12 with the initial concentration of 50 mg L^{-1} and contact time of 40 min. As shown in Fig. 8, an abrupt increase in the adsorption capacity was observed in the pH range of 2–4. Then the adsorption remained almost constant within the range of pH 4–12. Methylene blue exists in the form of positively charged ions in the aqueous solution. The solution pH would affect both aqueous chemistry and surface binding-sites of the adsorbents. The low adsorption efficiencies at lower pH may be explained by the fact that high concentration of H$^+$ would compete with dye ions for the vacant adsorption sites of the adsorbent, thereby inhibiting the dye adsorption. While at neutral and alkaline pH, adsorbents became negatively charged, which would greatly enhance the positively charged dye ions through electrostatic forces of attraction [23].

3.5.3. Adsorption kinetics

The effect of contact time on the amount of MB adsorbed was investigated at the initial concentrations of 20, 50 and 70 mg L^{-1}, respectively (A in Fig. 9). The rate of adsorption increased rapidly during the initial adsorption stage, and reached equilibrium after 40 min. The adsorption capacity increased with increasing the initial dye concentrations. This was due to the fact that there were more methylene blue molecules available at higher dye concentrations, which could provide a higher driving force to overcome the mass transfer resistance of the dye between the aqueous phases and the solid phases [24]. Thus, there were more collisions between methylene blue molecules and active sites on the adsorbent which was helpful for adsorption process [25].

To investigate the adsorption mechanism, pseudo-first-order and pseudo-second-order kinetic models were both studied to find the best fitted model for the

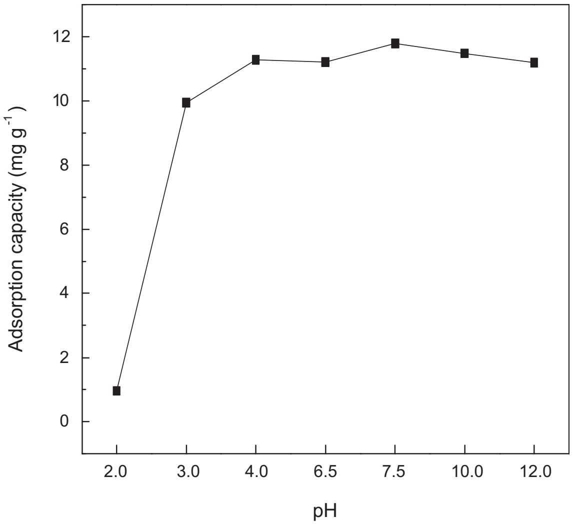

Fig. 8. Effect of initial pH on MB adsorption (T: 25 ± 2℃, MB = 50 mg L^{-1}, t = 40 min.).

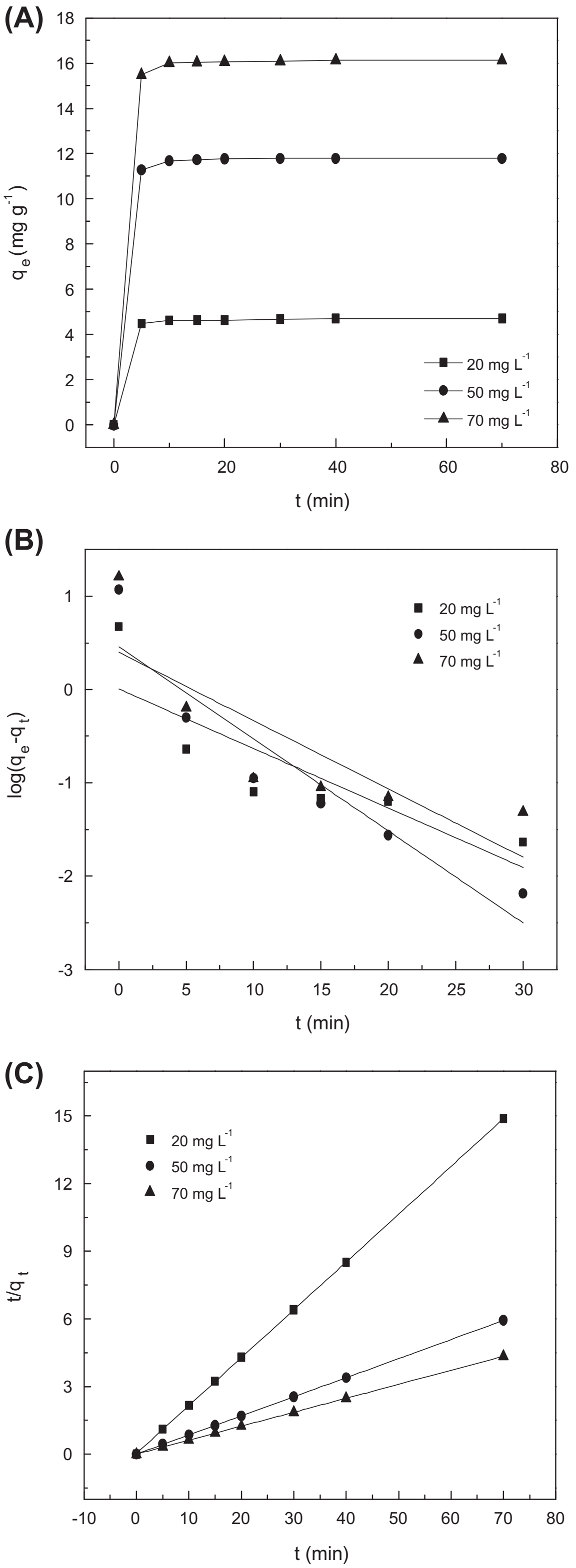

Fig. 9. (A) Adsorption kinetics of MB adsorption with different initial MB concentrations, (B) linear plot of log $(q_e - q_t)$ vs. t, and (C) linear plot of t/q_t vs. t.

experimental data. The pseudo-first-order Lagergren equation is given by Lagergren [26]:

$$\log(q_e - q_t) = \log q_e - \frac{k_1 t}{2.303} \tag{5}$$

where k_1 is the pseudo-first-order rate constant (min^{-1}), q_e and q_t are the amounts of dye adsorbed (mg g^{-1}) at equilibrium and at time t (min). The pseudo-second-order model can be expressed as [27]:

$$\frac{t}{q_t} = \frac{1}{k_2 q_e^2} + \frac{t}{q_e} \tag{6}$$

where k_2 ($\text{g mg}^{-1}\,\text{min}^{-1}$) is the rate constant of the pseudo-second-order adsorption.

Kinetic constants obtained by linear regression for two models are listed in Table 4. These parameters were calculated for the adsorption of synthesized ferrite. Eq. (5) shows a linear relationship between $\log(q_e - q_t)$ and t. Linear regression calculation can obtain the values of the rate constant k_1 and the equilibrium adsorption capacity q_e. The low correlation coefficient (R^2) value suggests that the experimental results did not fit the pseudo-first-order model. Whereas, it was found that the plot of t/q_t against time gave a straight line. Good correlation was observed and the pseudo-second-order kinetic model with correlation coefficient values close to unity. The result indicates that the adsorption system followed predominantly the second-order rate model and the overall process appeared to be controlled by chemisorptions [28].

3.5.4. *Adsorption isotherm*

The equilibrium adsorption isotherm is fundamental in describing the interactive behavior between solutes and adsorbent, which is important for the design of adsorption system. In the present study, two common isotherms—Langmuir and Freundlich—were employed. The linear forms of the Langmuir and Freundlich models are represented by the following equations [29,30]:

$$\text{Langmuir:}\ \frac{C_e}{q_e} = \frac{1}{bq_m} + \frac{C_e}{q_m} \tag{7}$$

$$\text{Freundlich:}\ \log q_e = \log k_f + \frac{1}{n}\log C_e \tag{8}$$

where q_e is the amount adsorbed at equilibrium (mg g^{-1}), C_e is the equilibrium concentration of the

Table 4
Adsorption kinetic parameters for MB adsorption on synthesized ferrite

	Pseudo-first-order			Pseudo-second-order		
C_0 (mg L^{-1})	k_1 (min^{-1})	$q_{e,\mathrm{cal}}$ (mg g^{-1})	R^2	k_2 (mg g^{-1} min^{-1})	$q_{e,\mathrm{cal}}$ (mg g^{-1})	R^2
20	0.15	1.01	0.6574	1.09	4.71	0.9999
50	0.23	2.86	0.8516	0.86	11.81	0.9999
70	0.17	2.50	0.6027	0.61	16.15	0.9999

MB (mg L^{-1}), constant b is related to the energy of adsorption (L mg^{-1}), and q_m is the Langmuir monolayer adsorption capacity (mg g^{-1}). When C_e/q_e is plotted against C_e, straight line with slope $1/q_m$ is obtained (insert in Fig. 10). k_f (mg g^{-1}) and n are Freundlich constants. The isotherm parameters for the MB adsorption are listed in Table 5. The linearization of the equations was $y = 0.03024x + 0.1848$, and the value of correlation coefficient (R^2) was 0.9969. The q_m value for the adsorption of MB was 33.07 mg g^{-1}. As seen from Table 5, regression correlation coefficient by the Langmuir model was much higher than that of the Freundlich model. Thus, the Langmuir model was more suitable for describing the adsorption equilibrium of MB in adsorption process. Moreover, the essential characteristics of the Langmuir isotherm can be expressed in terms of a dimensionless constant separation factor R_L given by the following equation [31]:

$$R_L = \frac{1}{1 + bC_o} \tag{9}$$

where b (L mg^{-1}) is the Langmuir constant and C_0 (mg L^{-1}) is the initial concentration in the liquid phase. The value of R_L indicates the shape of the isotherm to be either unfavorable ($R_L > 1$), linear ($R_L = 1$), favorable ($0 < R_L < 1$), or irreversible ($R_L = 0$) [32]. R_L values obtained from the adsorption process were in the range of 0.0204–0.238, indicating the adsorption was a favorable process.

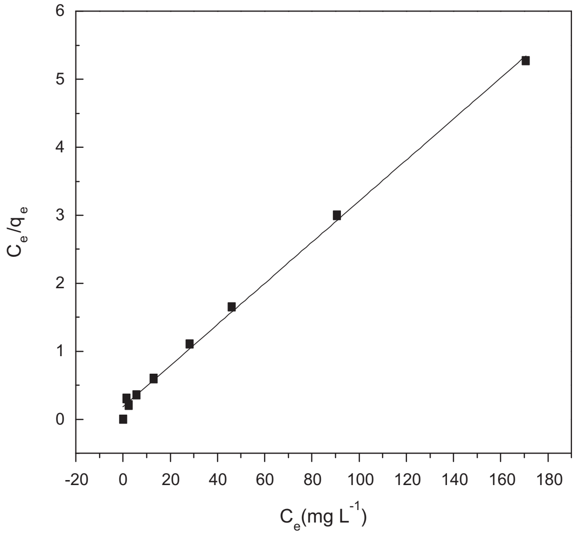

Fig. 10. Langmuir Isotherms of MB adsorption on synthesized ferrite.

Table 5
Isotherm parameters for MB adsorption on synthesized ferrite

Langmuir model				Freundlich model		
b (L mg^{-1})	q_m (mg g^{-1})	R^2	R_L	n	K_F	R^2
0.16	33.07	0.9969	0.0204–0.238	2.91	7.06	0.7905

4. Conclusions

In this study, pure spinel ferrite was successfully synthesized from two kinds of spent pickling liquors via microwave hydrothermal method. The crystalline single phase of the synthesized ferrite was good (V_{SPLA}:V_{SPLB} = 1:1), and it showed soft magnetic property with high saturation magnetization (Ms) of 48.57 emu/g. TCLP result proved that the product was highly stable in acid conditions. The low activation energy of 5.54 kJ/mol confirmed that the microwave hydrothermal method is environmentally friendly and it is economic technology to co-treat industrial wastewater. The process of adsorption was best described by the pseudo-second-order kinetic model. The equilibrium of adsorption of MB onto ferrite was suitably described by Langmuir models with a monolayer adsorption capacity of 33.07 mg g^{-1}. To use in technology design, it is to ensure that spinel ferrite has better properties under the certain conditions (V_{SPLA}:V_{SPLB} = 1:1, the reaction temperature range 150–180 ℃). Besides, the synthesized ferrite could be used as an effective dye adsorbent with adsorption capacity of 11.78 mg/g after 40 min.

Acknowledgments

This study was carried out under the key subject of Shanghai Municipality (S30109), as well as been supported by National Nature Science Foundation of China Nos. 50704023, 50974086, and 51274138 Shanghai University Excellence Youth Fund. This study was also funded by China Scholarship Council.

List of symbols

A — the intercept
C_0 (mg/L) — initial MB concentration
C_e (mg/L) — equilibrated MB concentration
D — the average crystalline size
k — the specific reaction rate constant
m (g) — the mass of the adsorbent (dry)
Q — the activation energy
q (mg/g) — adsorption capacity
R — the ideal gas constant
T — the absolute temperature
V (L) — The volume of added solution
β — the full width at half maximum (FWHM) of the diffraction peaks
θ — the Bragg's angle
λ — the wavelength of Cu Kα

References

[1] V.S.T. Ciminelli, A. Dias, H.C. Braga, Simultaneous production of impurity-free water and magnetite from steel pickling liquors by microwave-hydrothermal processing, Hydrometallurgy 84 (2006) 37–42.

[2] I. Mohai, J. Szépvölgyi, Treatment of particulate metallurgical wastes in thermal plasmas, Chem. Eng. Processing: Process Intensif. 44 (2005) 225–229.

[3] Z. Sun, L. Liu, D.Z. Jia, W. Pan, Simple synthesis of $CuFe_2O_4$ nanoparticles as gas-sensing materials, Sens. Actuators B Chem. 125 (2007) 144–148.

[4] N. Nasrallah, M. Kebir, Z. Koudri, M. Trari, Photocatalytic reduction of Cr(VI) on the novel hetero-system $CuFe_2O_4$/CdS, J. Hazard. Mater. 185 (2011) 1398–1404.

[5] R. Rahimi, H. Kerdari, M. Rabbani, M. Shafiee, Synthesis, characterization and adsorbing properties of hollow $Zn–Fe_2O_4$ nanospheres on removal of Congo red from aqueous solution, Desalination 280 (2011) 412–418.

[6] S. Yang, Y. Guo, N. Yan, D. Wu, H. He, J. Xie, Z. Qu, J. Jia, Remarkable effect of the incorporation of titanium on the catalytic activity and SO_2 poisoning resistance of magnetic Mn–Fe spinel for elemental mercury capture, Appl. Catal. B Environ. 101 (2011) 698–708.

[7] D. Chen, J. Hou, L.H. Yao, H.-M. Jin, G.R. Qian, Z.P. Xu, Ferrite materials prepared from two industrial wastes: Electroplating sludge and spent pickle liquor, Sep. Purif. Technol. 75 (2010) 210–217.

[8] J.H. Lee, C.K. Kim, S. Katoh, R. Murakami, Microwave-hydrothermal vs. conventional hydrothermal preparation of Ni- and Zn-ferrite powders, J. Alloys Comp. 325 (2001) 276–280.

[9] D. Chen, C.Y. Mei, L.H. Yao, H.M. Jin, G.R. Qian, Z.P. Xu, Flash fixation of heavy metals from two industrial wastes into ferrite by microwave hydrothermal co-treatment, J. Hazard. Mater. 192 (2011) 1675–1682.

[10] A.C. Sophia, K. Swaminathan, Assessment of the mechanical stability and chemical leachability of immobilized electroplating waste, Chemosphere 58 (2005) 75–82.

[11] Q. Xu, Y. Wei, Y. Liu, X. Ji, L. Yang, M. Gu, Preparation of Mg/Fe spinel ferrite nanoparticles from Mg/Fe-LDH microcrystallites under mild conditions, Solid State Sci. 11 (2009) 472–478.

[12] M. Erdem, F. Tumen, Chromium removal from aqueous solution by the ferrite process, J. Hazard. Mater. 109 (2004) 71–77.

[13] X. Hou, J. Feng, X. Liu, Y. Ren, Z. Fan, M. Zhang, Magnetic and high rate adsorption properties of porous $Mn_{1-x}Zn_xFe_2O_4$ $(0 <= x <= 0.8)$ adsorbents, J. Colloid Interface Sci. 353 (2011) 524–529.

[14] M.M. Rashad, R.M. Mohamed, M.A. Ibrahim, L.F.M. Ismail, E.A. Abdel-Aal, Magnetic and catalytic properties of cubic copper ferrite nanopowders synthesized from secondary resources, Adv. Powder Technol. 23 (2012) 315–323.

[15] I.H. Gul, A.Z. Abbasi, F. Amin, M. Anis-ur-Rehman, A. Maqsood, Structural, magnetic and electrical properties of $Co_{1-x}Zn_xFe_2O_4$ synthesized by co-precipitation method, J. Magn. Magn. Mater. 311 (2007) 494–499.

[16] X. Li, G. Wang, Low-temperature synthesis and growth of superparamagnetic $Zn_{0.5}Ni_{0.5}Fe_2O_4$ nanosized particles, J. Magn. Magn. Mater. 321 (2009) 1276–1279.

[17] C.J. Liu, X. Wang, Y. Wei, Y.F. Jiang, Y. Yang, Study on crystallization kinetics mechanism of soft-magnetic MnZn ferrite, Rare Metal Mat. Eng. 38 (2009) 515–519.

[18] Z.H. Yang, Z.Q. Gong, H.X. Li, Y.T. Ma, Y.F. Yang, Synthesis of Ni–Zn ferrite and its microstructure and magnetic properties, J. Central South Univ. Technol. 13 (2006) 618–623.

[19] G. Zhang, J. Qu, H. Liu, A.T. Cooper, R. Wu, $CuFe_2O_4$/activated carbon composite: A novel magnetic adsorbent for the removal of acid orange II and catalytic regeneration, Chemosphere 68 (2007) 1058–1066.

[20] X. Hou, J. Feng, Y. Ren, Z. Fan, M. Zhang, Synthesis and adsorption properties of sponge like porous $MnFe_2O_4$, Colloids Surf. A: Physicochem. Eng. Asp. 363 (2010) 1–7.

[21] H. Deng, L. Yang, G. Tao, J. Dai, Preparation and characterization of activated carbon from cotton stalk by microwave assisted chemical activation: Application in methylene blue adsorption from aqueous solution, J. Hazard. Mater. 166 (2009) 1514–1521.

[22] R. Wu, J. Qu, H. He, Y. Yu, Removal of azo-dye Acid Red B (ARB) by adsorption and catalytic combustion using magnetic $CuFe_2O_4$ powder, Appl. Catal. B: Environ. 48 (2004) 49–56.

[23] K. Gobi, M.D. Mashitah, V.M. Vadivelu, Adsorptive removal of Methylene Blue using novel adsorbent from palm oil mill effluent waste activated sludge: Equilibrium, thermodynamics and kinetic studies, Chem. Eng. J. 171 (2011) 1246–1252.

[24] A. Zümriye, Biosorption of reactive dyes by dried activated sludge: equilibrium and kinetic modelling, Biochem. Eng. J. 7 (2001) 79–84.

[25] L. Ai, J. Jiang, Fast removal of organic dyes from aqueous solutions by AC/ferrospinel composite, Desalination 262 (2010) 134–140.

[26] S. Lagergren, About the theory of so-called adsorption of soluble substances, Kungliga Svenska Vetenskapsakademiens Handlingar 24 (1898) 1–39.

[27] Y.S. Ho, G. McKay, Sorption of dye from aqueous solution by peat, Chem. Eng. J. 70 (1998) 115–124.

[28] S. Chatterjee, S. Chatterjee, B.P. Chatterjee, A.R. Das, A.K. Guha, Adsorption of a model anionic dye, eosin Y, from aqueous solution by chitosan hydrobeads, J. Colloid Interface Sci. 288 (2005) 30–35.

[29] I. Langmuir, The constitution and fundamental properties of solids and liquids. Part I. Solids, J. Amer. Chem. Soc. 38 (1916) 2221–2295.

[30] H.M.F. Freundlich, Over the adsorption in solution, Z. Phys. Chem. 57 (1906) 385–471.

[31] T.W. Webi, R.K. Chakravort, Pore and solid diffusion models for fixed-bed adsorbers, AIChE J. 20 (1974) 228–238.

[32] G. McKay, Adsorption of dyestuffs from aqueous solutions with activated carbon I: Equilibrium and batch contact-time studies, J. Chem. Technol. Biotechnol. 32 (1982) 759–772.